Spatiotemporal mode locking in quadratic nonlinear media

Article *in* PHYSICAL REVIEW E · August 2020

DOI: 10.1103/PhysRevE.102.022205

2 authors, including:

Mahmut Bağcı
Yeditepe University
8 PUBLICATIONS **19** CITATIONS

SEE PROFILE

Spatiotemporal mode locking in quadratic nonlinear media

Mahmut Bağcı*
Department of Computer Technology, Istanbul Bilgi University, Kozyatagi 34742, Istanbul, Turkey

J. Nathan Kutz
Department of Applied Mathematics, University of Washington, Seattle, Washington 98195-2420 USA

(Received 20 May 2020; accepted 21 July 2020; published 11 August 2020)

A theoretical model is developed to characterize spatiotemporal mode locking (ML) in quadratic nonlinear media. The model is based on the two-dimensional nonlinear Schrödinger equation with coupling to a mean term (NLSM) and constructed as an extension of the master mode-locking model. It is numerically demonstrated that there exists steady-state soliton solutions of the ML-NLSM model that are astigmatic in nature. A full stability analysis and bifurcation study is performed for the ML-NLSM model, and it is manifest that spatiotemporal ML of the astigmatic steady-state solutions is possible in quadratic nonlinear media.

DOI: 10.1103/PhysRevE.102.022205

I. INTRODUCTION

Mode locking (ML) is a commonly observed phenomenon in optical resonator cavities where nonlinear interactions in the cavity synchronize different cavity modes to produce localized and stable light pulses. Such nonlinear synchronization processes where first observed shortly after the invention of the laser [1–4]. Modern mode-locking lasers [5,6] are now a mature, turn-key technology commonly used in many branches of science and commercial applications [7,8]. Traditionally, the key nonlinear process responsible for synchronizing cavity modes is a cubic Kerr nonlinearity or intensity-dependent index of refraction. Its interaction with linear dispersion and the cavity gain-loss dynamics are the basis of the canonical *master mode-locking equation* [9,10], which characterizes the equilibration of the pulse energy, and the consequent balance of nonlinearity and dispersion in forming stable pulses [11–13]. More recently, spatiotemporal ML has been considered for creating light-bullet structures in Kerr media [14–17]. In this work, we develop a theory of spatiotemporal ML in quadratic media and show that stable ML can be achieved. This provides an important extension of the mode-locking theoretical framework to a broader class of problems whose quadratic nonlinearities can be leveraged with orders of magnitude less power.

Spatiotemporal ML is difficult to achieve in practice due to the physical balances that must be achieved in both the spatial and temporal domains. Although ML has promoted a great deal of work in synchronizing temporal cavity modes, there has been relatively little work in understanding how to coherently superimpose spatial modes or mode lock in the spatial domain. If both can be simultaneously synchronized, then spatiotemporal ML can be achieved. The work of Wright *et al.* [17], for instance, uses spatial filtering to achieve a variety of spatiotemporal ML states. In many applications, however, the leading nonlinear polarization effect in an optical material is quadratic. Quadratic materials are referred to as χ^2 materials, where χ^2 is the second-order susceptibility that describes second harmonic generation first experimentally observed by Franken *et al.* [18]. Indeed, until such observations [19], Maxwell's equations were thought to be linear. Pulse shaping in quadratic media was proposed early [20], with optical solitons theoretically predicted by Karamzin and Sukhorukov shortly after [21,22]. In Belashenkov *et al.* [23] and DeSalvo *et al.* [24], experiments in a χ^2 crystal demonstrated modulational instability and the self-defocusing phenomena typically observed in centro-symmetric χ^3 materials. In 1995, optical solitons in a quadratic bulk material were observed by Torruellas *et al.* [25], and existence of the solitons in a χ^2 waveguide were observed experimentally by Schiek *et al.* [26] in 1996. These original results have since been corroborated and extended in many follow-up experiments [27–32], demonstrating that quadratic solitons can exist in both the spatial and the temporal domains in waveguides or bulk materials [33–36]. One of the distinguished properties of a quadratic nonlinear medum is that it provides stable multidimensional pulse propagation without collapse in any dimension [33,34,37].

It is well known that the pulse dynamics in multidimensional nonresonant χ^2 materials cannot be generally described by nonlinear Schrödinger (NLS)-based equations [38–41]. Indeed, these dynamics are governed by generalized NLS systems with coupling to a mean term (hereafter denoted as NLSM systems, which are sometimes referred to as Benney-Roskes or Davey-Stewartson type) [42,43].

Benney and Roskes [42] first obtained NLSM equations in water of finite depth h and without surface tension in 1969. In 1974 Davey and Stewartson [43] reached an equivalent form of the NLSM equations by investigating the evolution of a 3D wave packet in water of finite depth. The integrability of NLSM systems was studied in 1975 by Ablowitz and

*bagcimahmut@gmail.com

Haberman [44] in the shallow water limit. In 1977 the results of Benney and Roskes were extended to include surface tension by Djordevic and Reddekopp [45]. Ablowitz *et al.* [38–40] derived from first-principles NLSM-type equations describing the evolution of the electromagnetic field in quadratic nonlinear media. Recently it was demonstrated [46] that optical wave collapse can be arrested in the NLSM system by adding an external potential (lattice) to the model.

The NLSM system is physically derived from an expansion of the slowly varying wave amplitude in the first and second harmonics of the fundamental frequency and a mean term that corresponds to the zeroth harmonic. This system describes the nonlocal-nonlinear coupling between a dynamic field that is related with the first harmonic and a static field that is related with the zeroth harmonic [47]. The general NLSM system is given by [39,40,48]

$$iu_t + \nabla^2 u + |u|^2 u - \rho u\phi = 0, \tag{1a}$$

$$\phi_{xx} + \nu\phi_{yy} = (|u|^2)_{xx} \tag{1b}$$

where $u(x,t)$ is the normalized amplitude of the envelope of the normalized static electric field (which is associated with the first harmonic). The parameter ρ is a coupling constant that comes from the combined optical rectification and electro-optic effects modeled by the $\phi(x,y)$ field, and ν is the coefficient that comes from the anisotropy of the material.

Given the long history of the NLSM model and its broad applications to fluids and optics alike, we build on the pioneering optical work of Ablowitz and co-workers to characterize ML in quadratic nonlinear media. Specifically, we modify the model to include the critical gain-loss dynamics that are a hallmark feature of mode-locking systems. Indeed, ML is manifestation of a broader class of damp-driven systems which are common across the sciences. For instance, ML is also observed in rotating detonation engines [49,50], where energy balances are similar to mode-locking laser cavities [51,52]. Thus we develop a mode-locking theory for the NLSM optical systems, denoted ML-NLSM, by including bandwidth limited, saturating gain, and cavity losses to model the overall mode-locking dynamics which is capable of producing stable, 2D-soliton like solutions in the NLSM model. A full stability analysis and bifurcation study is performed for this new ML-NLSM model. Our ML-NLSM model is the quadratic, 2D analog of the master mode-locking theory of Haus.

The paper is outlined as follows: In Sec. II the ML-NLSM is presented and steady-state solutions (fundamental solitons) of the model are obtained numerically. In Sec. III the mode-locking dynamics of the fundamental solitons are explored by direct numerical simulations of our derived ML-NLSM governing equations. Section IV provides a stability analysis which details the linear stability of the fundamental spatiotemporal solitons. Results of the study are discussed in Sec. V.

II. (2 + 1)D NLSM SYSTEMS

Our theoretical considerations begin by considering the NLSM model [39,40,48] in Eq. (1). The model is modified to account for cavity losses and a bandwidth-limited, saturating gain term which is canonical in ML models for lasers [11]. The ML-NLSM model in (2 + 1) dimensions is given by

$$iu_t + \frac{D}{2}\nabla^2 u + \beta|u|^2 u - \rho\phi u = iRu, \tag{2a}$$

$$\phi_{xx} + \nu\phi_{yy} = (|u|^2)_{xx}, \tag{2b}$$

where R is the gain-loss operator given by

$$R = g(t)(1 + \tau\nabla^2) - \gamma - p|u|^4 + \alpha\phi \tag{3}$$

with the time-depended gain saturation dynamics $g(t)$ given by

$$g(t) = \frac{2g_0}{1 + ||u||^2/e_0}. \tag{4}$$

In the formulation, $u(x,y,t)$ is a function of time t and the transverse variables x and y. D denotes the average diffraction coefficient. The evolution dynamics is coupled to the $\phi(x,y)$ field. The parameter β represents the strength of the cubic nonlinearity, and p represents the strength of the quintic self-phase modulation term. The coupling parameter ρ describes the combined optical rectification and electro-optic effects. In the operator R, all parameters are positive. These include the gain bandwidth τ and the linear attenuation parameter γ. The dynamic gain $g(t)$ depends on the input pump strength $g_0 > 0$, cavity saturation energy e_0, and the total cavity energy (L^2 norm) $\|u\|^2 = \iint |u|^2\,dx\,dy$ where integration is performed over the entire space of x and y [16].

The ML-NLSM equation (2) along with its solutions and dynamics represents the primary contribution of this paper. The model has a number of features of note. First, the model is a (2 + 1)-dimensional model in electric field envelop $u(x,t)$. For $\rho = 0$ and $R = 0$ the (2 + 1) NLS equation has solutions that exhibit finite time blowup of solutions [53]. This behavior is regularized by both the coupling to ϕ and the gain-loss dynamics given by the operator R. Importantly, this model includes the material anisotropy through the parameter ν. Of primary interest is to determine if localized ML solutions exist for this system, thus allowing the ML-NLSM to support quadratic spatiotemporal solitons. Such soliton-like solutions are considered in the following subsections using recently developed numerical methods for finding steady-state solutions of partial differential equations.

A. Numerical solutions using the squared operator method (SOM)

In order to obtain the fundamental soliton solutions of the (2 + 1)D ML-NLSM, we use a modification of the computational algorithm called the *squared operator method* (SOM) [54]. The method is based on iterating differential equations whose linearization operators are squares of those of the original equations, together with an acceleration technique. The scheme of the method is outlined in what follows.

Substituting the ansatz $u = U(x,y)\exp(i\mu t)$ into the model (2), we get the operator

$$\mathbf{L}_0\mathbf{u} = \frac{D}{2}\nabla^2 U + \beta|U|^2 U + i\gamma U - ig(t)(1 + \tau\nabla^2) + ip|U|^4 U - \rho\phi U - i\alpha\phi U - \mu U,$$

$$\phi_{xx} + \nu\phi_{yy} = (|U|^2)_{xx}, \tag{5}$$

where μ is propagation constant. Separating the operator $\mathbf{L}_0$ into its real and imaginary parts gives the following suboperators:

$$T1 = \mathrm{Re}\left\{\mathcal{F}^{-1}\left[\frac{\mathcal{F}(\mathbf{L}_0\mathbf{u})}{K^2+c}\right]\right\},$$
$$T2 = \mathrm{Im}\left\{\mathcal{F}^{-1}\left[\frac{\mathcal{F}(\mathbf{L}_0\mathbf{u})}{K^2+c}\right]\right\}, \tag{6}$$

where $\mathcal{F}$ symbolizes Fourier transformation, $k = (k_x, k_y)$ are wave numbers in the x and y directions, respectively, $K^2 = k_x^2 + k_y^2$, and c is a parameter for parametrizing the numerical scheme. Decomposing the amplitude into its real and imaginary parts $U = u(x, y) + iv(x, y)$ and inserting into $\mathbf{L}_0\mathbf{u}$, we get the two suboperators

$$\begin{aligned} L_{\mathrm{Re}} &= \frac{D}{2}\nabla^2 u + \beta(u^3 + uv^2) - \gamma v + g(t)(1+\tau\nabla^2)v \\ &\quad - p(u^4 v + 2u^2 v^3 + v^5) - \rho\phi u + \alpha\phi v - \mu u, \\ L_{\mathrm{Im}} &= \frac{D}{2}\nabla^2 v + \beta(v^3 + u^2 v) - \gamma u - g(t)(1+\tau\nabla^2)u \\ &\quad + p(u^5 + 2u^3 v^2 + uv^4) - \rho\phi v - \alpha\phi u - \mu v. \end{aligned} \tag{7}$$

Taking partial derivatives of these new operators with respect to both u and v gives the matrix components

$$\begin{aligned} R_{11} &= \frac{\partial L_{\mathrm{Re}}}{\partial u}(T1), \quad R_{12} = \frac{\partial L_{\mathrm{Re}}}{\partial v}(T2), \\ R_{21} &= \frac{\partial L_{\mathrm{Im}}}{\partial u}(T1), \quad R_{22} = \frac{\partial L_{\mathrm{Im}}}{\partial v}(T2). \end{aligned} \tag{8}$$

Using the elements of this matrix, the final operator is defined as

$$\mathbf{L}_1\mathbf{u} = R_{11} + R_{12} + i(R_{21} + R_{22}). \tag{9}$$

After the operator is defined, the iteration scheme is implemented as follows:

$$\begin{aligned} U_{n+1} &= U_n - \left\{\mathcal{F}^{-1}\left[\frac{\mathcal{F}(\mathbf{L}_1\mathbf{u})}{K^2+c}\right]\right\}\Delta t, \\ \mu_{n+1} &= \mu_n + \|u\cdot T1 + v\cdot T2\|\Delta t, \\ \phi_{n+1} &= \mathcal{F}^{-1}\left[\frac{k_x^2\mathcal{F}(|U_n|^2)}{k_x^2 + \nu k_y^2}\right]. \end{aligned} \tag{10}$$

This numerical algorithm is iterated from an initial guess until the error $E = \sqrt{\|U_{n+1} - U_n\|^2 + |\mu_{n+1} - \mu_n|} < 10^{-6}$. This algorithm has been demonstrated to be efficient and accurate in computing localized solutions for a wide range of nonlinear PDEs [54]. It is also effective for the ML-NLSM model proposed here in generating the desired mode-locked spatiotemporal states of interest.

B. Numerical existence of the fundamental solitons

The SOM algorithm is used to compute a steady-state solution (fundamental soliton) of the ML-NLSM (2). Once the solution is obtained, it can be used for the linear stability properties of the solitons. In what follows, the following set of

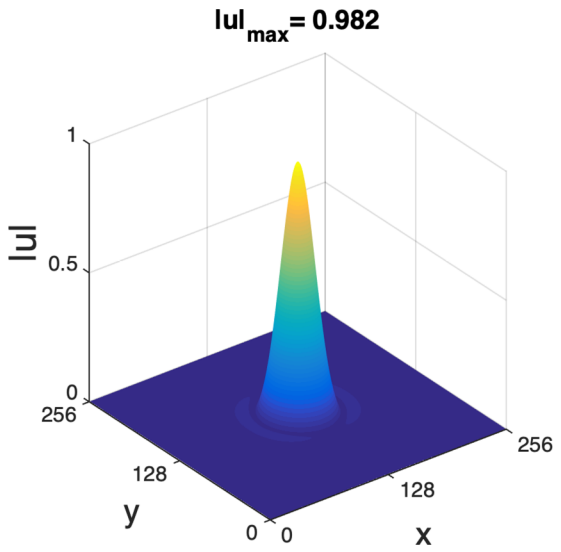

FIG. 1. Fundamental soliton that is obtained when $\rho = 0.5$, $\nu = 1.5$, $c = 5$, and $\Delta t = 0.1$.

base parameters are used. Unless otherwise specified, we set

$$\begin{aligned} &(D, \beta, \gamma, g_0, E_0, \tau, p, \alpha, \mu) \\ &\quad = (1, 1, 1, 4.88, 1, 0.08, 0.5, 1, 1), \end{aligned} \tag{11}$$

and we set the coupling constant to $\rho = 0.5$ and the asymmetry parameter to $\nu = 1.5$, typical values corresponding to the propagation of focused beams in potassium niobate ($KNbO_3$) [48].

With these parameters, the numerical convergence to the fundamental soliton (steady-state solution) is shown in Fig. 1 for the parameter values $\rho = 0.5$ and $\nu = 1.5$ in the ML-NLSM system when $c = 5$ and $\Delta t = 0.1$ in the algorithm. In addition, we have found that the fundamental soliton solution can be obtained for $0 \leqslant \rho \leqslant 1.9$ when $\nu = 1.5$ with suitable c and Δt parameters.

It is noteworthy that, as demonstrated in previous studies [46,47], due to the anisotropy of the ML-NLSM system, steady-state solutions do not possess radial symmetry. In other words, the ML-NLSM model generates astigmatic fundamental solitons. To explore the level of astigmatism in the solitions, we define

$$e = \frac{\text{radius along } y \text{ axis}}{\text{radius along } x \text{ axis}} \tag{12}$$

as a measure of astigmatism. When $e = 1$, the solution corresponds to a radially symmetric fundamental soliton, and $e < 1$ and $e > 1$ correspond to a soliton that is relatively wider along the x and y axes, respectively. Thus it takes on an elliptical shape for $e \neq 1$.

Contour images of fundamental solitons are plotted in Fig. 2 for $\rho = 0$, $\rho = 0.5$, and $\rho = 1$, respectively. It can be seen from Fig. 2 that as ρ increases, the contours of the fundamental soliton become more astigmatic along the x axis. On the other hand, we observe that as the anisotropy coefficient ν increases (for a fixed ρ), the fundamental soliton become less astigmatic along the x axis, and after a threshold

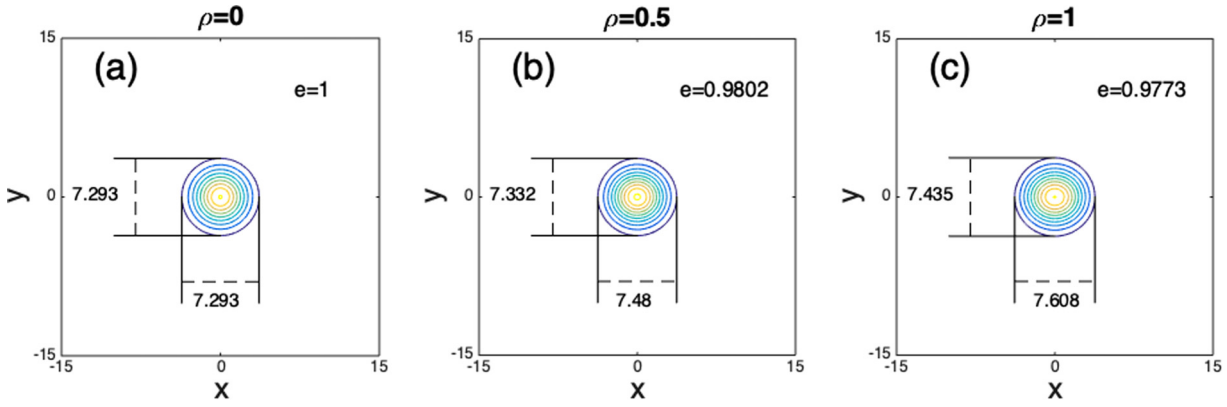

FIG. 2. Contour image of the fundamental soliton for (a) $\rho = 0$; (b) $\rho = 0.5$; (c) $\rho = 1$. All solitons are obtained when $\nu = 1$.

value of ν (i.e., when $\nu \geqslant 1.3$ and $\rho = 0.5$) the solitons become relatively wider along the y axis.

III. DYNAMICS OF FUNDAMENTAL SOLITON

To investigate the dynamics of the ML-NLSM solitons, we directly simulate Eq. (2) for long times. A finite-difference discretization scheme is used in the spatial domain and the solution is advanced in time with a fourth-order Runge-Kutta method. We plot 3D views and profiles of the solitons versus the propagation time during the evolution (from $t = 0$ to $t = t_{\max}$). Stable (mode-locked) soliton solutions should nearly preserve their mode shape, profile, and peak amplitude over time. Figure 3 shows the evolution of the fundamental soliton (obtained in Fig. 1) from $t \in [0, 200]$ with a numerical time step of $dt = 0.001$. Snapshots of the evolution dynamics are plotted for $t = 0$, $t = 50$, $t = 100$, $t = 150$, and $t = 200$.

As can be seen from the Fig. 3, the profile of the evolved soliton (upper panels) is preserved, and the peak amplitude of the fundamental soliton oscillates with relatively small amplitude during the evolution. At the end of the simulation for $t = 200$, the mode shape of the evolved soliton (lower panels) is shown to be preserved. These results demonstrate that the considered soliton is mode-locked in this parameter regime.

Similar to the fundamental steady-state solutions, mode-locked evolution of the pulses can be achieved starting from seeded white noise. In Fig. 4 evolution of the very low-amplitude initial solutions from $t \in [0, 200]$ is depicted, the parameters used are identical to those of Fig. 3.

Both the fundamental solitons and white-noise initial solutions are mode-locked when $0 \leqslant \rho < 0.9$, $\nu = 1.5$, and $\alpha = 1$ in the ML-NLSM model. When $\rho \geqslant 0.9$, the peak amplitude of the fundamental solitons decreases after a short time of evolution and the solitons decay into radiation modes and is not self-supporting. Decay of the fundamental soliton

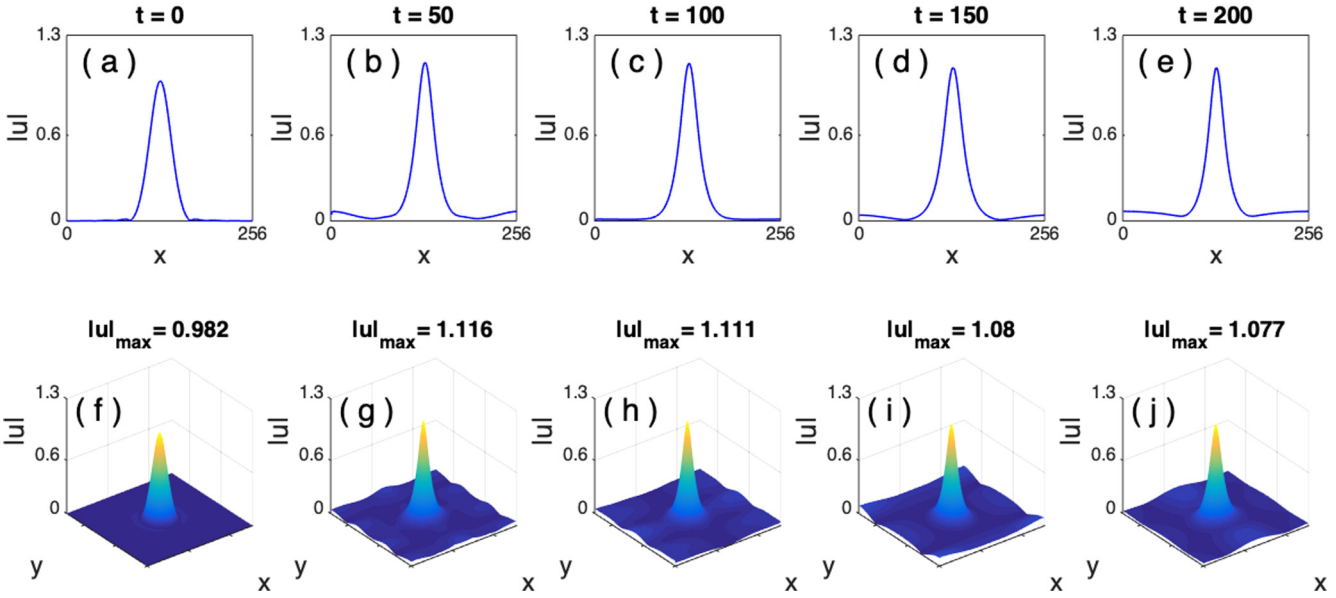

FIG. 3. Nonlinear evolution of the fundamental soliton from $t = 0$ to $t = 200$. Five snapshots of the soliton captured at different propagation times. Profile of the evolved soliton along the x axis is plotted (upper panels) (a) when $t = 0$, (b) when $t = 50$, (c) when $t = 100$, (d) when $t = 150$, (e) when $t = 200$; and the corresponding 3D view of the evolved soliton is plotted (lower panels) (f) when $t = 0$, (g) when $t = 50$, (h) when $t = 100$, (i) when $t = 150$, and (j) when $t = 200$. The fundamental soliton is obtained when $\rho = 0.5$, $\nu = 1.5$, and $\alpha = 1$.

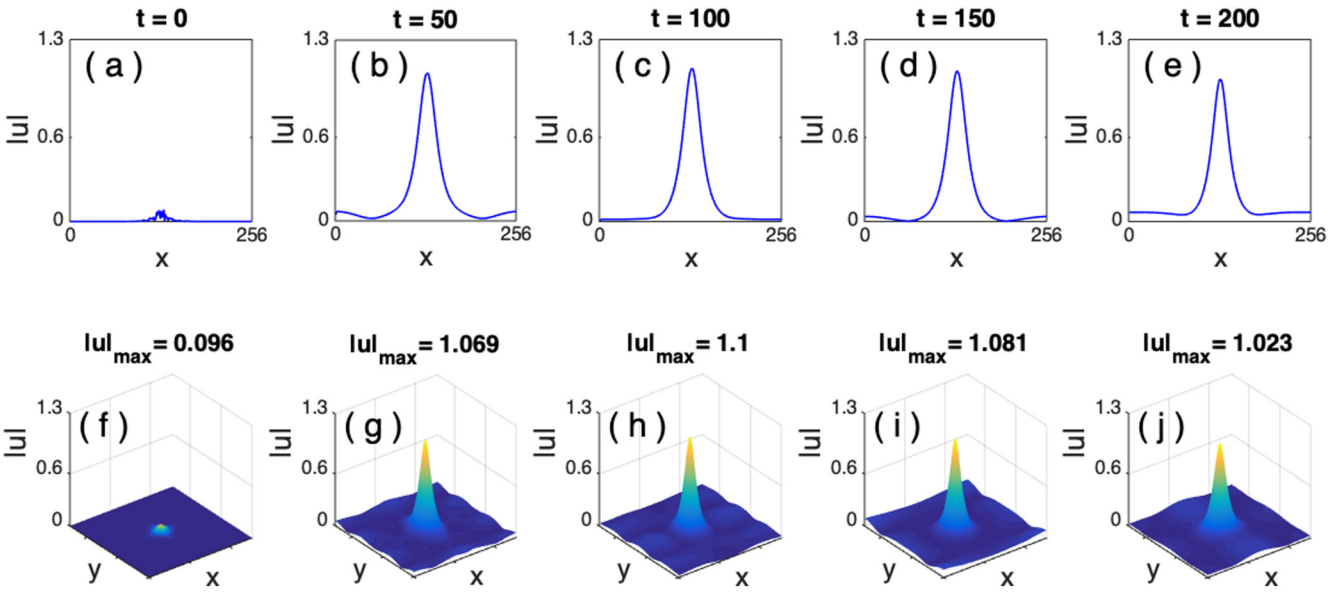

FIG. 4. Nonlinear evolution of the mode-locked pulses starting from seeded white noise. Five snapshots of the solution captured at different propagation times. Profile of the evolved pulse along the x axis is plotted (upper panels) (a) when $t = 0$, (b) when $t = 50$, (c) when $t = 100$, (d) when $t = 150$, (e) when $t = 200$; and the corresponding 3D view of the evolved pulse is plotted (lower panels) (f) when $t = 0$, (g) when $t = 50$, (h) when $t = 100$, (i) when $t = 150$, and (j) when $t = 200$ when $\rho = 0.5$, $\nu = 1.5$, and $\alpha = 1$.

computed for $\rho = 1$, $\nu = 1.5$, and $\alpha = 1$ is plotted in Fig. 5. It is obvious that the soliton can not stay mode-locked during the evolution since the amplitude of the soliton decreases significantly during the evolution (see Fig. 5, upper panels) and the mode shape is no longer preserved during evolution (see Fig. 5, lower panels).

In addition, it has seen that the α parameter (which shows a quadratic polarization effect) plays an important role in ML of the fundamental solitons. Fundamental solitons that are obtained when $\rho = 0.5$ and $\nu = 1.5$ are stable for $0.7 \leqslant \alpha < 2.1$, while for $\alpha = 0$ and $\rho > 0$ in the ML-NLSM model, the fundamental solitons decay into radiation modes and no ML occurs. Decay of the fundamental soliton for $\rho = 0.5$, $\nu = 1.5$, and $\alpha = 0$ is showed in Fig. 6. One can easily see that peak amplitude of the soliton decreases sharply after a short propagation distance (see Fig. 6, upper panels), and the soliton is dispersed away entirely during the evolution (see Fig. 6, lower panels).

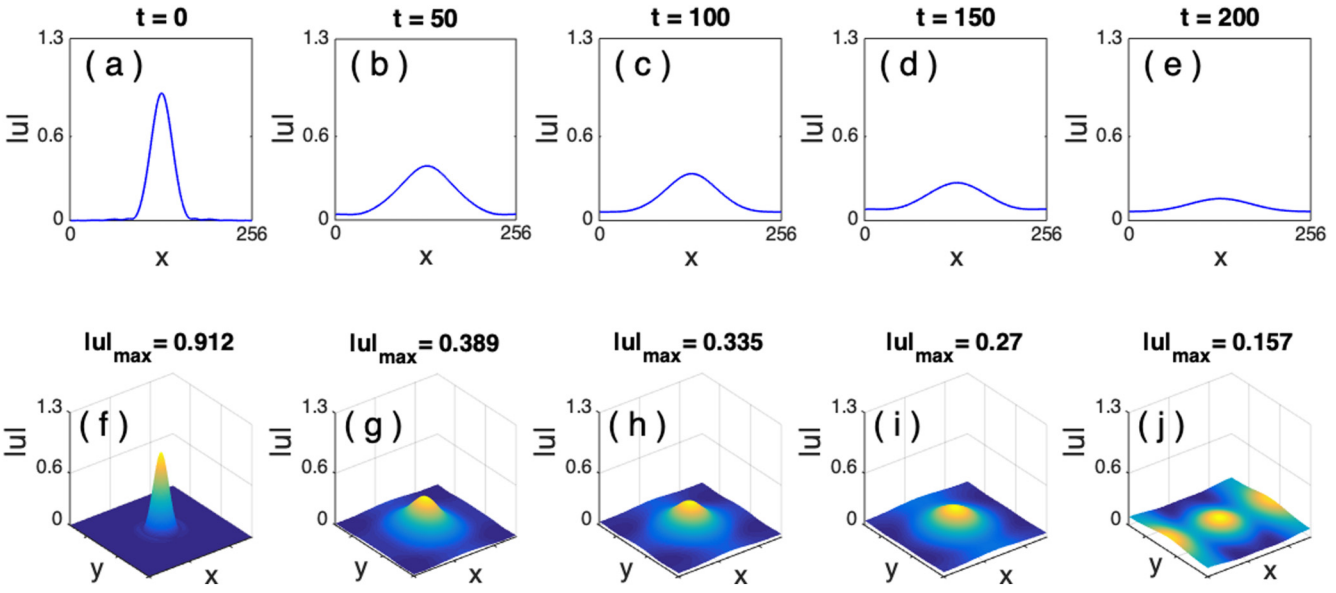

FIG. 5. Decay of the fundamental soliton, that is obtained when $\rho = 1$, $\nu = 1.5$, and $\alpha = 1$, is demonstrated with five snapshots of the soliton captured at different propagation times. Profile of the evolved soliton along the x axis is plotted (upper panels) (a) when $t = 0$, (b) when $t = 50$, (c) when $t = 100$, (d) when $t = 150$, (e) when $t = 200$; and the corresponding 3D view of the evolved soliton is plotted (lower panels) (f) when $t = 0$, (g) when $t = 50$, (h) when $t = 100$, (i) when $t = 150$, and (j) when $t = 200$.

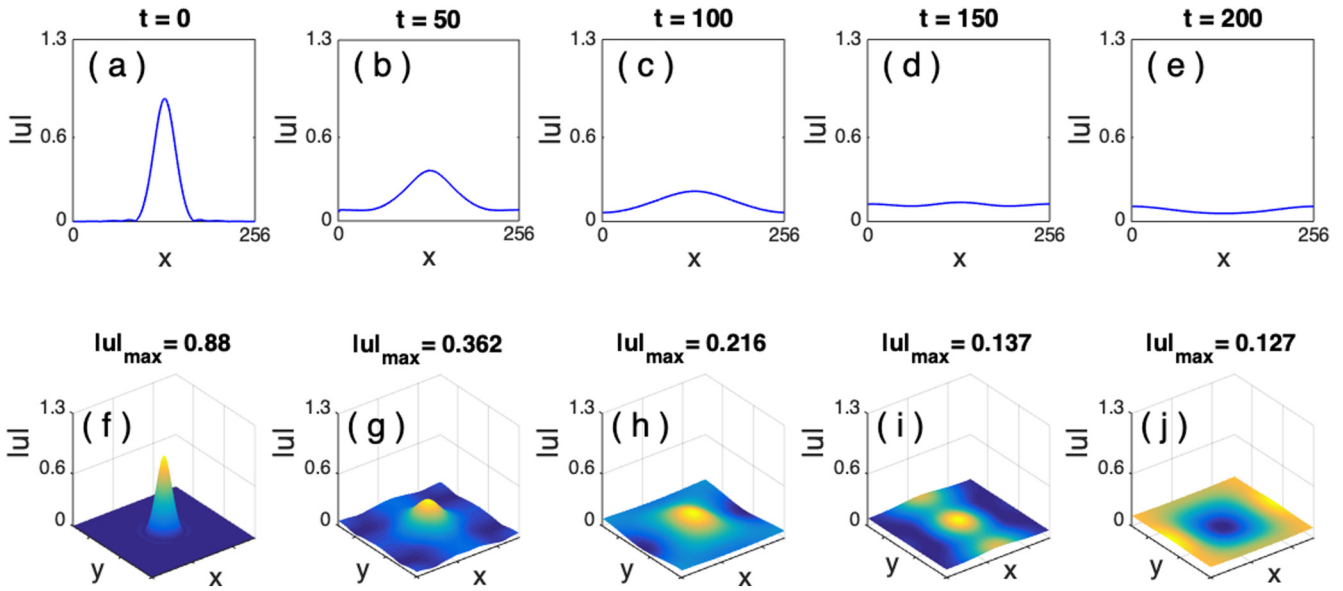

FIG. 6. Decay of the fundamental soliton, which is obtained when $\rho = 0.5$, $\nu = 1.5$, and $\alpha = 0$, is demonstrated with five snapshots of the soliton captured at different propagation times. Profile of the evolved soliton along the x axis is plotted (upper panels) (a) when $t = 0$, (b) when $t = 50$, (c) when $t = 100$, (d) when $t = 150$, (e) when $t = 200$; and the corresponding 3D view of the evolved soliton is plotted (lower panels) (f) when $t = 0$, (g) when $t = 50$, (h) when $t = 100$, (i) when $t = 150$, and (j) when $t = 200$.

Furthermore, we have seen that decaying of the fundamental solitons can be arrested (or delayed) by increasing the value of the anisotropy coefficient ν. As a special case we have increased the value of ν from 1 to 4 and plot the evolution of the fundamental soliton that is obtained for $\rho = 1$ and $\alpha = 1$ in Fig. 7. It is clearly seen that although the soliton, which is obtained for $\nu = 1$, does not blow up in finite time, it cannot be considered as robust since the amplitude of the soliton decreases significantly after $t = 10$ [see Fig. 7(a)] and finally (at $t = 200$) it decays to radiation modes [see Fig. 7(b)]. To improve the stability of the considered soliton, we increase the value of ν to $\nu = 2$ and $\nu = 4$ and depict the nonlinear evolution of the soliton for each case in Figs. 7(c) and 7(e), respectively. We observe that the decay of the soliton is delayed when $\nu = 2$ [see Figs. 7(c) and 7(d)] and decay of the soliton is prevented when $\nu = 4$ [see Fig. 7(e) and 7(f)].

It should be pointed out that, in real optical systems, increasing the anisotropy parameter ν may not be used to arrest solitons' decay in some cases, since ρ and ν parameters are fixed values depending on the type of material that is considered. However, the anisotropy ν can be applied to improve the stability of solitons in the range of real physical parameter regime.

IV. LINEAR STABILITY ANALYSIS

A standard way for determining stability is to calculate the spectrum of linearization of the model (2) about the fundamental soliton solutions computed with the SOM technique. By denoting

$$u = e^{-i\theta t}[u_0(x, y) + \tilde{u}(x, y, t)], \tag{13}$$

where $u_0(x, y)$ is the fundamental soliton, θ is propagation constant and $\tilde{u} \ll 1$ is the infinitesimal perturbation. If the perturbation $\tilde{u}$ decays to zero, then the fundamental soliton is considered to be linearly stable. Inserting the perturbed solution into Eq. (2), we get the linearized system for $\tilde{u}$ by neglecting small terms of the second order $O(\tilde{u}^2)$:

$$\begin{aligned}\tilde{u}_t = {} & i\theta\tilde{u} + i\frac{D}{2}\nabla^2\tilde{u} + i\beta\left(2|u_0|^2\tilde{u} + u_0^2\tilde{u}^*\right) - \gamma\tilde{u} \\ & + g(t)(1+\tau\nabla^2)\tilde{u} - p\left(3|u_0|^4\tilde{u} + 2|u_0|^2u_0^2\tilde{u}^*\right) \\ & - i\rho\phi\tilde{u} + \alpha\phi\tilde{u}.\end{aligned} \tag{14}$$

Separating the fundamental soliton and the perturbations into real and imaginary parts as

$$u_0 = a_0 + ib_0, \quad \tilde{u} = R_0e^{\lambda t} + iI_0e^{\lambda t}, \tag{15}$$

we obtain $\tilde{u}_t = \lambda\tilde{u}$, and substituting u_0, $\tilde{u}$ into the system (14) results in the eigenvalue problem

$$\mathbf{AV} = \lambda\mathbf{V}, \tag{16}$$

where

$$A = \begin{pmatrix} F_R & G_I \\ G_R & F_I \end{pmatrix}, \quad V = \begin{pmatrix} R_0 \\ I_0 \end{pmatrix}.$$

If the real part of the λ is positive, the fundamental soliton is unstable. The eigenvalues of $\mathbf{A}$ can be calculated numerically with finite difference discretization of the spatial domain. Note that the matrix coefficients of $\mathbf{A}$ are given by

$$\begin{aligned}F_R = {} & -2\beta a_0b_0 - \gamma + g(t)(1+\tau\nabla^2) - p\left(5a_0^4 + b_0^4 + 6a_0^2b_0^2\right) \\ & + \alpha\phi - \frac{4g_0}{(1+||u||^2)^2}(1+\tau\nabla^2)a_0 * a_0, \\ G_I = {} & -\left[\frac{D}{2}\nabla^2 + \beta\left(a_0^2 + 3b_0^2\right) + 4p\left(a_0^3b_0 + a_0b_0^3\right) + \theta - \rho\phi\right]\end{aligned}$$

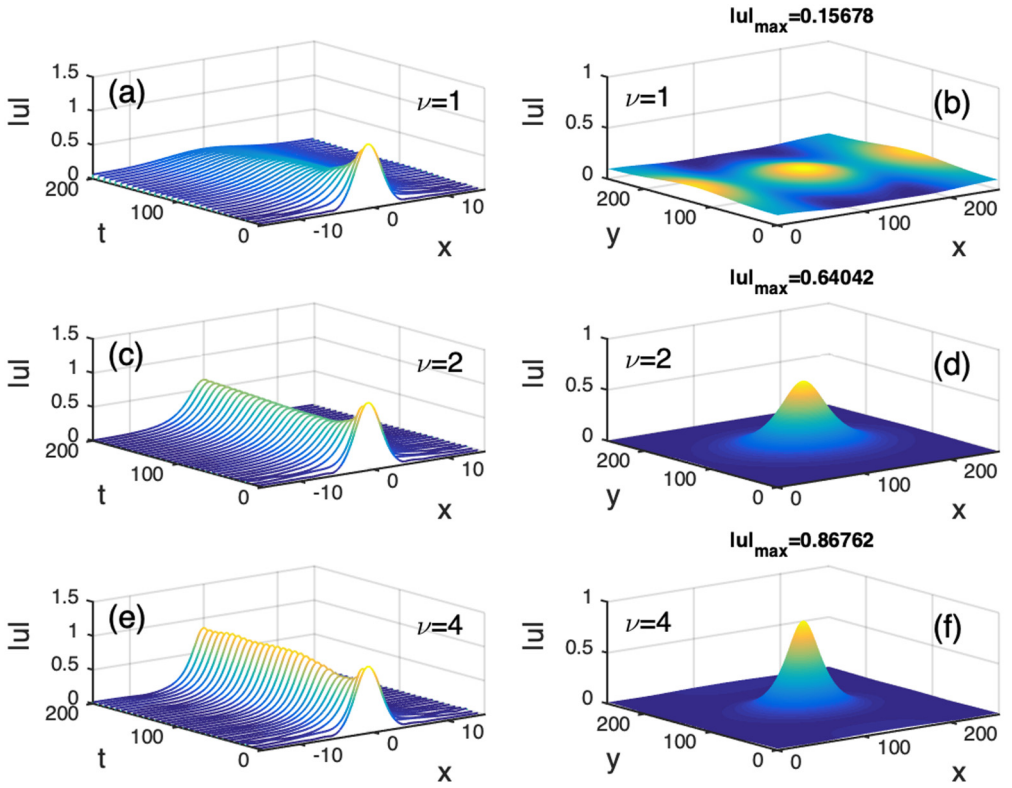

FIG. 7. Nonlinear evolution of the fundamental soliton for larger anisotropy coefficients (a) when $\nu = 1$, (c) when $\nu = 2$, and (e) when $\nu = 4$. 3D view of the soliton after evolution at $t = 200$ (b) when $\nu = 1$, (d) when $\nu = 2$, and (f) when $\nu = 4$. All fundamental solitons are obtained for $\rho = 1$ and $\alpha = 1$.

$$
\begin{aligned}
&-\frac{4g_0}{(1+||u||^2)^2}(1+\tau\nabla^2)a_0 * b_0,\\
F_I &= 2\beta a_0 b_0 - \gamma + g(t)(1+\tau\nabla^2) - p\left(a_0^4 + 5b_0^4 + 6a_0^2 b_0^2\right)\\
&+\alpha\phi - \frac{4g_0}{(1+||u||^2)^2}(1+\tau\nabla^2)b_0 * b_0,\\
G_R &= \left[\frac{D}{2}\nabla^2 + \beta\left(3a_0^2 + b_0^2\right) - 4p\left(a_0^3 b_0 + a_0 b_0^3\right) + \theta - \rho\phi\right]\\
&-\frac{4g_0}{(1+||u||^2)^2}(1+\tau\nabla^2)a_0 * b_0. \qquad (17)
\end{aligned}
$$

The $*$ notation denotes the integral $a_0 * b_0 = \int_{-\infty}^{\infty} a_0(\tau)b_0(\tau)\,d\tau$, which results from the nonlocal behavior given by the saturated gain dynamics [55].

The linear spectra of fundamental solitons can be computed by evaluating the matrix **A**. In Fig. 8 the maximum real part of the eigenvalue spectra versus parameters ρ, ν, and α are plotted. In this analysis, we have changed parameters ρ, ν, and α one by one, when other parameters are fixed ($\rho = 0.5$, $\nu = 1.5$, and $\alpha = 1$). Figure 8 shows that when $0 \leqslant \rho < 0.9$, $0 \leqslant \nu \leqslant 5$, and $0.7 \leqslant \alpha \leqslant 2.1$, there is no eigenvalue with a positive real part in the spectrum of the model, thus showing these ML-NLSM solitons to be linearly stable. For $\rho \geqslant 0.9$, $\alpha < 0.7$, or $\alpha > 2.1$ [see Figs. 8(a)–8(c)] the maximum real part of eigenvalues are positive, which indicates that these fundamental solitons are linearly unstable. In addition, we have seen that similarly to being nonlinearly unstable, the fundamental soltions become linearly unstable when $\alpha = 0$ and $\rho > 0$.

V. CONCLUSION

The proposed ML-NLSM model has been formulated as an extension of the master mode-locking model by the addition of higher-order dispersion and quadratic electro-optic effects. This study reveals the potential of using quadratic nonlinear media to generate spatiotemporal mode-locked soliton states in a nonlinear optical system. Using modern computational methods we have shown that there exist steady-state soliton solutions of the ML-NLSM mode-locking model that are astigmatic in nature. Stability of the ML-NLSM states has been characterized by direct numerical simulation of the model as well as by linear stability arguments and computation of the spectra of the linearized operator. Both show that the soliton solutions of the ML-NSLM model have regions of stable spatiotemporal ML.

Specifically, it has been shown that when the coupling constant ρ (that comes from the combined optical rectification and electro-optic effects) is smaller than 0.9, there is no eigenvalue with a positive real part in the spectrum of linearization of the ML-NLSM model, thus showing that the fundamental solitons in this region are stable, mode-locking states that act as attractors. The nonlinear stability of the fundamental solitons have been examined with direct simulations of the ML-NLSM model, and the results demonstrate that for $\rho < 0.9$, the fundamental solitons' profile are preserved and

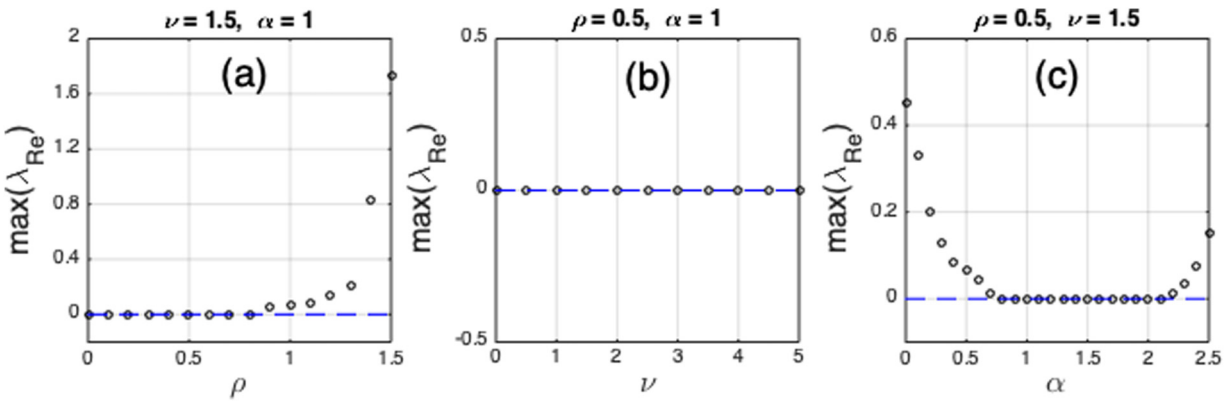

FIG. 8. The maximum real part of the eigenvalue spectra versus parameters ρ, ν, and α (a) when ρ is varied, $\nu = 1.5$, and $\alpha = 1$; (b) when ν is varied, $\rho = 0.5$, and $\alpha = 1$; and (c) when α is varied, $\rho = 0.5$, and $\nu = 1.5$.

the peak amplitude of the solitons oscillates relatively small amplitude during the nonlinear evolution, which means stable ML is achieved during the evolution.

In addition, it has seen that the α parameter (which shows a quadratic polarization effect) has a critical importance for mode-locking operation in the ML-NLSM model. Specifically for $\alpha = 0$ and $\rho > 0$, the fundamental solitons decay to radiation modes, and none of the ML-NLSM soliton states stay mode-locked. In conclusion, we have constructed the ML-NLSM model as a modification of the master mode-locking model and demonstrated the possibility of ML of astigmatic steady-state solutions in the quadratic nonlinear media.

ACKNOWLEDGMENTS

M.B. was supported by TUBITAK under International Postdoctoral Research Fellowship Programme under Grant No. 1059B191600743.

[1] M. DiDomenico Jr., Small-signal analysis of internal (coupling-type) modulation of lasers, J. Appl. Phys. **35**, 2870 (1964).
[2] L. E. Hargrove, R. L. Fork, and M. A. Pollack, Locking of He–Ne laser modes induced by synchronous intracavity modulation, Appl. Phys. Lett. **5**, 4 (1964).
[3] A. Yariv, Internal modulation in multimode laser oscillators, J. Appl. Phys. **36**, 388 (1965).
[4] P. W. Smith, Mode-locking of lasers, Proc. IEEE **58**, 1342 (1970).
[5] H. A. Haus, Mode-locking of lasers, IEEE J. Sel. Top. Quant. Elec. **6**, 1173 (2000).
[6] I. N. Duling III and M. L. Dennis, *Compact Sources of Ultrashort Pulses* (Cambridge University Press, Cambridge, 1995).
[7] A. E. Siegman, *Lasers* (University Science Books, Sausalito, CA, 1986).
[8] A. Weiner, in *Ultrafast Optics*, edited by G. D. Boreman, Wiley Series in Pure and Applied Optics Vol. 72 (John Wiley & Sons, New York, 2011).
[9] H. A. Haus, J. G. Fujimoto, and E. P. Ippen, Structures for additive pulse mode locking, J. Opt. Soc. Amer. B Opt. Phys. **8**, 2068 (1991).
[10] H. A. Haus, J. G. Fujimoto, and E. P. Ippen, Analytic theory of additive pulse mode- locking and Kerr lens mode-locking, IEEE J. Quant. Elec. **28**, 2086 (1992).
[11] J. N. Kutz, Mode-locked soliton lasers, SIAM Rev. **48**, 629 (2006).
[12] M. J. Ablowitz and T. P. Horikis, Pulse dynamics and solitons in mode-locked lasers, Phys. Rev. A **78**, 011802(R) (2008).
[13] M. J. Ablowitz and T. P. Horikis, Solitons in normally dispersive mode-locked lasers, Phys. Rev. A **79**, 063845 (2009).
[14] M. O. Williams and J. N. Kutz, Spatial mode-locking of light bullets in planar waveguide arrays, Opt. Express **17**, 18320 (2009).
[15] M. O. Williams and J. N. Kutz, Light-bullet routing and control with planar waveguide arrays, Opt. Express **18**, 11671 (2010).
[16] E. Ding, K. Luh, and J. N. Kutz, Stability analysis of cavity solitons governed by the cubic-quintic Ginzburg-Landau equation, J. Phys. B. At. Mol. Phys. **44**, 065401 (2011).
[17] L. G. Wright, D. N. Christodoulides, and F. W. Wise, Spatiotemporal mode-locking in multimode fiber lasers, Science **358**, 94 (2017).
[18] P. A. Franken, A. E. Hill, C. W. Peters, and G. Weinreich, Generation of Optical Harmonics, Phys. Rev. Lett. **7**, 118 (1961).
[19] J. A. Armstrong, N. Bloembergen, J. Ducuing, and P. S. Pershan, Interactions between light waves in a nonlinear dielectric, Phys. Rev. **127**, 1918 (1962).
[20] L. A. Ostrovskii, Self-action of light in crystals, ZhETF Pis'ma **5**, 331 (1967) [JETP Lett. **5**, 272 (1967)].
[21] Y. N. Karamzin and A. P. Sukhorukov, Nonlinear interaction of diffracted light beams in a medium with quadratic nonlinearity: Mutual focusing of beams and limitation on the efficiency of optical frequency converters, ZhETF Pis'ma Red. **20**, 734 (1974) [Sov. Phys. JETP Lett. **20**, 339 (1974)].
[22] Y. N. Karamzin and A. P. Sukhorukov, Mutual focusing of high-power light beams in media with quadratic nonlinearity, Zh. Eksp. Teor. Fiz. **68**, 834 (1975) [Sov. Phys. JETP **41**, 414 (1976)].
[23] N. R. Belashenkov, S. V. Gagarski, and M. V. Inochkin, Nonlinear refraction of light on second-harmonic generation, Opt. Spectrosc. **66**, 806 (1989).

[24] R. Desalvo, D. J. Hagan, M. Sheik-Bahae, and G. Stegeman, Self-focusing and self-defocusing by cascaded second-order effect in KTP, Opt. Lett. **17**, 28 (1992).
[25] W. E. Torruellas, Z. Wang, D. J. Hagan, E. W. VanStryland, G. I. Stegeman, L. Torner, and C. R. Menyuk, Observation of Two-Dimensional Spatial Solitary Waves in a Quadratic Medium, Phys. Rev. Lett **74**, 5036 (1995).
[26] R. Schiek, Y. Baek, and G. I. Stegeman, One-dimensional spatial solitary waves due to cascaded second-order nonlinearities in planar waveguides, Phys. Rev. E **53**, 1138 (1996).
[27] R. A. Fuerst, B. L. Lawrence, W. E. Torruellas, and G. I. Stegeman, Beam reshaping by use of spatial solitons in the quadratic nonlinear medium KTP, Opt. Lett. **22**, 19 (1997).
[28] R. A. Fuerst, D. M. Baboiu, B. L. Lawrence, W. E. Torruellas, G. I. Stegeman, S. Trillo, and S. Wabnitz, Spatial Modulational Instability and Multisolitonlike Generation in a Quadratically Nonlinear Optical Medium, Phys. Rev. Lett. **78**, 2756 (1997).
[29] B. Costantini, C. D. Angelis, A. Barthelemy, B. Bourliaguet, and V. Kermene, Collisions between type II two-dimensional quadratic solitons, Opt. Lett. **23**, 424 (1998).
[30] V. Couderc, E. Lopez-Lago, C. Simos, and A. Barthelemy, Experiments in quadratic spatial soliton generation and steering in a noncollinear geometry, Opt. Lett. **26**, 905 (2001).
[31] E. Lopez-Lago, C. Simos, V. Couderc, A. Barthelemy, D. Artigas, and L. Torner, Efficiency of quadratic soliton generation, Opt. Lett. **26**, 1277 (2001).
[32] M. Bache and F. W. Wise, Type-I cascaded quadratic soliton compression in lithium niobate: Compressing femtosecond pulses from high-power fiber lasers, Phys. Rev. A **81**, 053815 (2010).
[33] L. Torner and A. P. Sukhorukov, Quadratic solitons, Opt. Photon. News **13**, 42 (2002).
[34] A. V. Buryak, P. D. Trapani, D. V. Skryabin, and S. Trillo, Optical solitons due to quadratic nonlinearities: From basic physics to futuristic applications, Phys. Rep. **370**, 63 (2002).
[35] D. Mihalache, D. Mazilu, B. A. Malomed, and F. Lederer, Stable vortex solitons supported by competing quadratic and cubic nonlinearities, Phys. Rev. E **69**, 066614 (2004).
[36] V. Lutsky and B. A. Malomed, One- and two-dimensional solitons supported by singular modulation of quadratic nonlinearity, Phys. Rev. A **91**, 023815 (2015).
[37] K. Hayata and M. Koshiba, Multidimensional Solitons in Quadratic Nonlinear Media, Phys. Rev. Lett. **71**, 3275 (1993).
[38] M. Ablowitz, G. Biondini, and S. Blair, Localized multi-dimensional optical pulses in non-resonant quadratic materials, Math. Comp. Sim. **56**, 511 (2001).
[39] M. Ablowitz, G. Biondini, and S. Blair, Multi-dimensional pulse propagation in non-resonant $\chi^{(2)}$ materials, Phys. Lett. A **236**, 520 (1997).
[40] M. Ablowitz, G. Biondini, and S. Blair, Nonlinear Schrödinger equations with mean terms in non-resonant multi-dimensional quadratic materials, Phys. Rev. E **63**, 046605 (2001).
[41] M. J. Ablowitz, *Nonlinear Dispersive Waves Asymptotic Analysis and Solitons* (Cambridge University Press, New York, 2011).
[42] D. J. Benney and G. J. Roskes, Wave instabilities, Stud. App. Math. **48**, 377 (1969).
[43] A. Davey and K. Stewartson, On three-dimensional packets of surface waves, Proc. R. Soc. A **338**, 101 (1974).
[44] M. J. Ablowitz and R. Haberman, Nonlinear Evolution Equation—Two and Three Dimensions, Phys. Rev. Lett. **35**, 1185 (1975).
[45] V. D. Djordevic and L. G. Reddekopp, On two-dimensional packets of capillary-gravity waves, J. Fluid Mech. **79**, 703 (1977).
[46] M. Bağcı, İ. Bakırtaş, and N. Antar, Lattice solitons in nonlinear Schrödinger equation with coupling-to-a-mean-term, Opt. Commun. **383**, 330 (2017).
[47] M. J. Ablowitz, İ. Bakırtaş, and B. Ilan, Wave collapse in a class of nonlocal nonlinear Schrödinger equations, Physica D **207**, 230 (2005).
[48] L. C. Crasovan, J. P. Torres, D. Mihalache, and L. Torner, Arresting Wave Collapse by Wave Self-Rectification, Phys. Rev. Lett. **91**, 063904 (2003).
[49] J. Koch, M. Kurosaka, C. Knowlen, and J. N. Kutz, Mode-locked rotating detonation waves: Experiments and a model equation, Phys. Rev. E **101**, 013106 (2020).
[50] J. Koch, M. Kurosaka, C. Knowlen, and J. N. Kutz, Multi-scale physics of rotating detonation engines: Autosolitons and modulational instabilities, arXiv:2003.06655.
[51] S. Namiki, E. P. Ippen, H. A. Haus, and X. Y. Charles, Energy rate equations for mode-locked lasers, JOSA B **14**, 2099 (1997).
[52] F. Li, P. Wai, and J. N. Kutz, Geometrical description of the onset of multi-pulsing in mode-locked laser cavities, JOSA B **27**, 2068 (2010).
[53] M. J. Landman, G. C. Papanicolaou, C. Sulem, and P. L. Sulem, Rate of blowup for solutions of the nonlinear Schrödinger equation at critical dimension, Phys. Rev. A **38**, 3837 (1988).
[54] J. Yang and T. I. Lakoba, Universally-convergent squared-operator iteration methods for solitary waves in general nonlinear wave equations, Stud. App. Math. **118**, 153 (2007).
[55] B. G. Bale, E. Farnum, and J. N. Kutz, Theory and simulation of passive multifrequency mode-locking with waveguide arrays, IEEE J. Quant. Electron. **44**, 976 (2008).